ARMA 13-222

Seismic and aseismic motions generated by large scale fluid injections in a deep Granite massif

Cornet, F.H.
Institut de physique du Globe-Strasbourg, France

This paper was prepared for presentation at the 47th US Rock Mechanics / Geomechanics Symposium held in San Francisco, CA, USA, 23-26 June 2013.

ABSTRACT: Large scale hydraulic stimulations have been conducted at various depths on the geothermal site of Soultz-sous-forêts, in eastern France. In all cases these stimulations have generated microseismic activity which has been monitored with both a surface and a downhole network. This monitoring has shown that depending upon the relative magnitude of the pore pressure with respect to the local minimum principal stress magnitude, four different mechanisms control flow of water in such granite masses: diffusion through a poro-elastic rock mass or diffusion in preferential directions controlled either by slip on preexisting fractures, by the development of fresh fracture zones or by hydraulic fracturing. More importantly, this diffusion process induces large scale non seismic motions that, in turn, influence the seismic activity, in particular when injection stops.

1. THE EUROPEAN EXPERIMENTAL GEO-THERMAL PROJECT AT SOULTZ (FRANCE)

The European Experimental geothermal site at Soultz in eastern France has been ongoing since 1987 [1]. The site is located in the Rhine graben where a regional heat flux anomaly is associated with a 100°/km vertical thermal gradient in the local 1500 m thick sedimentary cover. Below the sedimentary cover, granite is encountered but the temperature gradient drops to a few degrees Celsius per km, outlining the existence of a large scale convective cell through the local fault system (fig. 1).

The objective of the project has been to stimulate hydraulically the natural fracture system so as to develop an artificial geothermal reservoir producing flow rates consistent with an electrical power production close to 2 Mw. The produced water was to be re-injected at depths where temperatures of the order of 200°C are encountered, i.e. about 5,000 m.

The reservoir development has been conducted in two different stages. The first one, from 1992 to 1997, involved two boreholes (GPK1 and GPK2) reaching a 3600 m depth, with large scale hydraulic stimulations and a 4 months circulation test. Then GPK2 was deepened to 5,000 m and two new deviated wells (GPK3 and GPK4) were drilled down to 5 km (fig. 2) [1, 2].

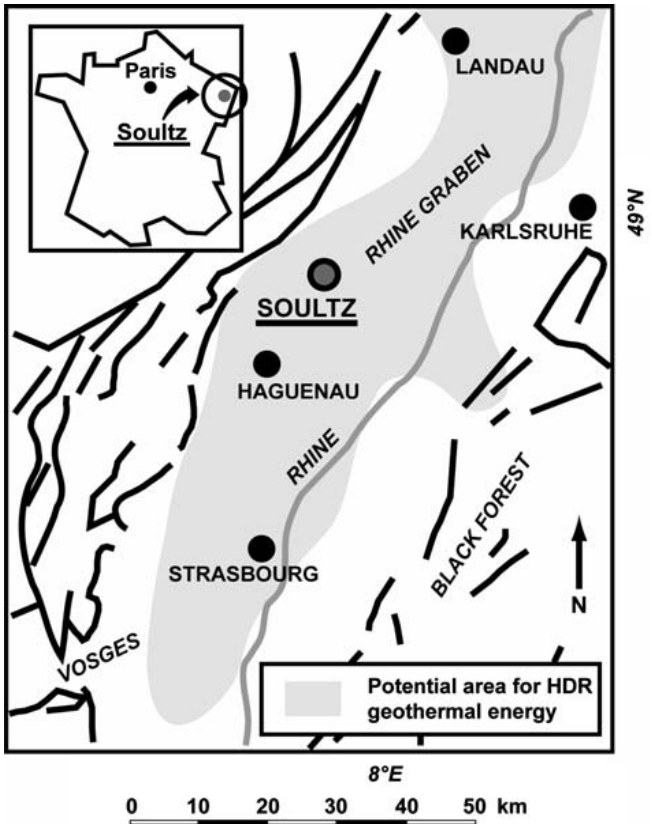

Fig. 1. Location of Soultz geothermal site in the Rhine graben.

The downhole distance between GPK4 and GPK2 is about 600 m whilst GPK3 is some 300 m away from both GPK2 and GPK4. The three wells are within a plane orientated roughly parallel to the maximum horizontal principal stress direction.

Various stimulations have been conducted at depths greater than 4,400 m and electricity production has been on-going since 2008. We discuss here observations associated with the stimulations of GPK1 and GPK2.

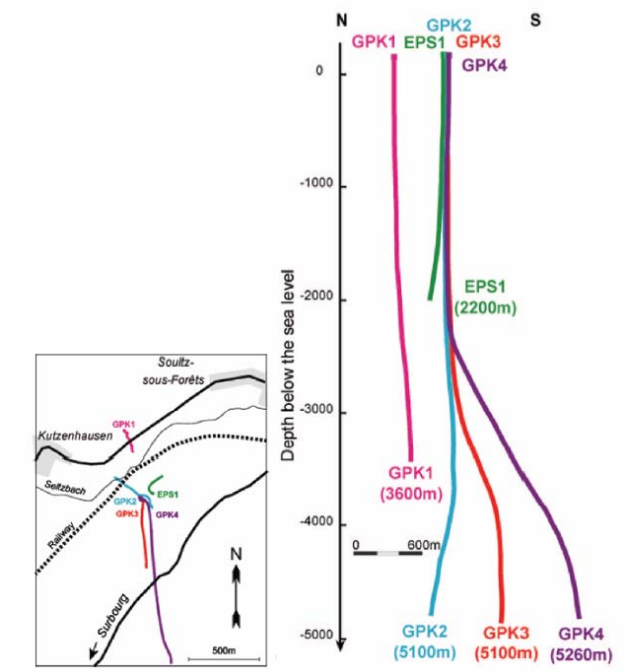

Fig. 2. Geometry of the various wells at Soultz

The first hydraulic stimulation, in GPK1, was conducted in an open hole section between 2850 m and 3400 m. Water injection proceeded with 6 10^{-3} m^3/s step wise flow rates increments every 48 h (fig. 5), from 6 10^{-3} m^3/s to 36 10^{-3} m^3/s, for a total injected volume equal to about 25,000 m^3 [3,9].

The local stress field is presently well constrained by an integrated analysis of hydraulic tests (shut-in pressure determination), drilling induced fractures orientation, thermal and compressive breakouts and focal mechanisms of induced seismicity [4, 5, 6, 7]. In the granite, the maximum horizontal principal stress is orientated N 170 ± 10°E and is sub-equal to the vertical (principal) stress component ($\sigma_H = (1 \pm 0.05)\ \sigma_v$), whilst the minimum horizontal principal stress component is slightly larger than half the vertical component ($\sigma_h = 0.535\ \sigma_v$). But various zones of local stress heterogeneity associated with preexisting fractures have been identified, with local principal stress direction rotations reaching up to 30° [4].

All hydraulic stimulations have been monitored with a seismic network, which has evolved over the years. For the 1993-1995 stimulations, seismic monitoring was conducted through two separated downhole and surface seismic networks that did not share the same clock. The downhole network [8], deployed at the top of the granite, involved four 4 components stations sampled at 5 KHz. The surface network [9] involved three permanent 3 components, 0.5 Hz, stations sampled at 150 Hz and located respectively 2.5 km, 6.5 km and 7 km from the site. In addition, fourteen stations were deployed only during stimulations and were sampled at 180 Hz. Since 2000, an integrated network of both downhole (5 stations sampled at 5 KHz) and surface stations (17 short periods stations sampled at 180 Hz) has been used [10].

Initially, the velocity models used for events location determinations included P and S sonic logs run within the boreholes together with calibration shots. These data were later complemented by seismic profiles conducted with both P and S vibrators located at various positions on ground.

During the stimulations, spinner (flow rate) logs were run to detect changes in hydraulic conductivity of the various fractures (e.g. fig. 3).

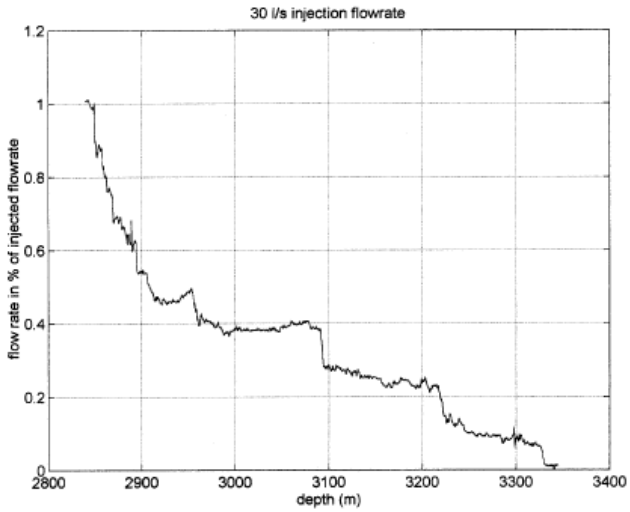

Fig. 3 Flow rate (spinner) log run in GPK1 during the 1993 stimulation. Horizontal axis is depth, vertical axis is percentage of total flow injected in the well (here 30 10^{-3} m^3/s) [11].

Note the significant (50 %) flow loss within the top 50 m of the open hole, and then the four main flow zones for this 30 l/s well head injection rate. For the 6 l/s injection rate, less than 10% flow losses occurred above 2900 m. This is further discussed in section 5.

2. SEISMIC ACTIVITY INDUCED DURING THE 1993 GPK1 HYDRAULIC STIMULATION

Whilst the surface network recorded 166 events during the 1993 stimulation of GPK1, the downhole network detected over 20 000 events. This is consistent with the fact that many signals were associated with small sources with only high frequency content that got undetected by the distant low frequency surface sensors.

As discussed by Sileny et al. [12], various failure mechanisms are associated with fluid stimulation and only double couple, shear events generate signals with low enough frequencies for being detected by distant, short periods (0.5 to 2 Hz) sensors.

Horizontal and vertical projections of events locations as determined from the downhole network are shown on figures 4 and 5.

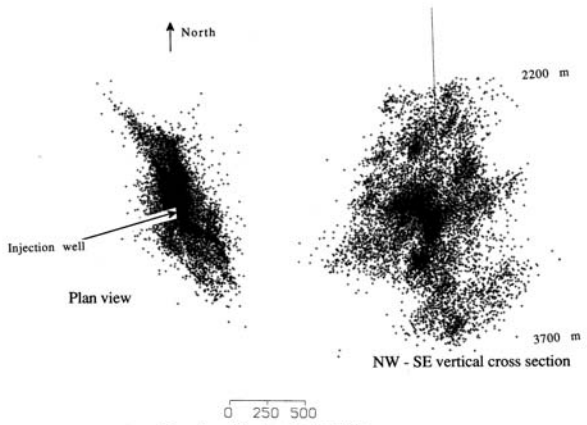

Fig. 4 Horizontal (left) and vertical (right) projections of microseismic events detected with the downhole network. The vertical projection is orientated N 150°E, i.e. parallel to the direction of the maximum horizontal extension of the cloud.

On figure 4, the vertical projection of event locations exhibits clearly marked linear limits, rather than an ovoidal shape. It illustrates the role of preexisting structures on the water percolation pattern.

Figure 5 (top) illustrates the change in shape of the seismic cloud with injection flow rate. When the wellhead injection pressure stabilizes slightly above 10 MPa whilst the injection flow rate keeps increasing, the seismic cloud starts growing upward, a feature consistent with hydraulic fracture propagation in a homogeneous material [13].

A second noticeable feature is the change in geometry of the seismic cloud growth, depending on the relative value of the injection pressure with respect to the minimum principal stress magnitude. Where the water pressure in the well is slightly larger than the local minimum principal stress magnitude, the growth of the seismic cloud is grossly in the N-S direction (fig. 5.b), i.e. parallel to the maximum horizontal principal stress direction. Where the water pressure in the well is slightly smaller than the local minimum principal stress magnitude, the growth of the seismic cloud is 24° to the west of the maximum horizontal principal stress direction [5]. This geometry has been determined from a statistical analysis of event locations through the 3 point method proposed by Fehler et al. [14]. It corresponds to the main trend of the seismic cloud but other secondary directions are also observed.

However, for wellbore pressures smaller than 8 MPa, i.e. values smaller than 80 % of the minimum principal stress magnitude observed when the injection flow rates are smaller than 18 l/s, the growth of the microseismic cloud remains axi-symmetrical with respect to the borehole axis.

These various geometries are discussed in section 5.

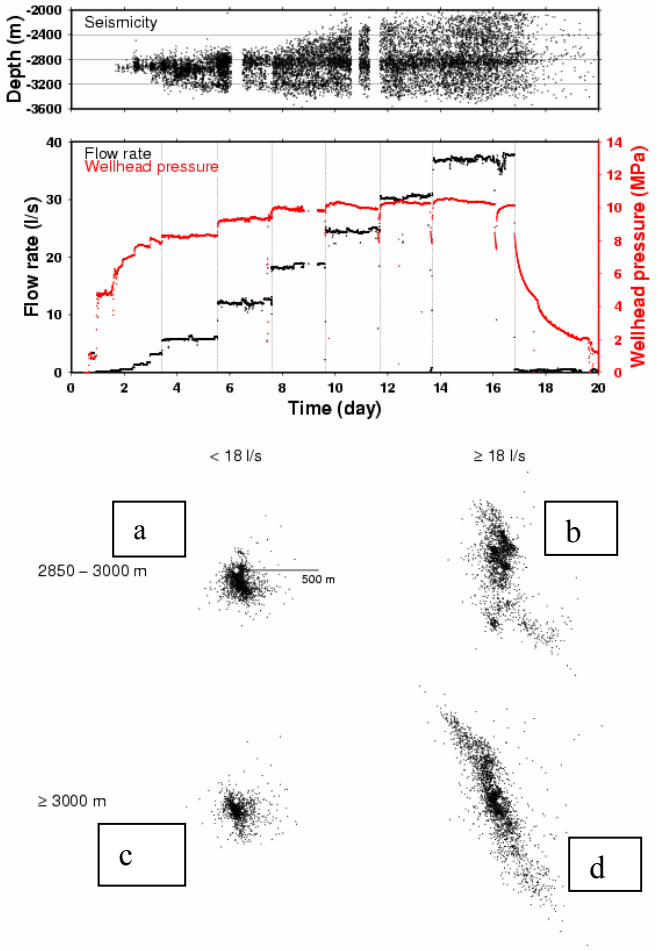

Fig. 5. Growth of the seismic cloud during the GPK1 stimulation. Top view is the vertical extension of the cloud with time. The four lower plots correspond respectively to horizontal projections between 2850 m and 3000 m (a and b) and depths greater than 3000 m (c and d). The left plots (a and c) correspond to injection flow rates smaller than 18 10^{-3} m^3/s whilst the plots on the right (b and d) correspond to flow rates larger than or equal to 18 10^{-3} m^3/s.

3. DIRECT AND INDIRECT EVIDENCE OF ASEISMIC MOTIONS INDUCED BY THE 1993 GPK1 HYDRAULIC STIMULATION

Acoustic imaging logs have been run before and after the 1993 GPK1 stimulation. They provide means to measure the amount of slip that has occurred on some of the fractures [9]. These results are then compared to evaluations of slip that can be derived from multiplet

analysis [15]. A multiplet is a seismic source that repeats itself over time. Simple source models provides means to evaluate the amount of slip that has occurred each time a source slips [16, 17] and the cumulated slip value provides an indirect estimate of the total slip that has occurred at this source location. It may be compared then to the value determined directly from UBI logs.

3.1. Results from Acoustic Imaging Logs

With this borehole wall imaging tool, an ultrasonic pulse is sent in a given azimuth, then reflects at the borehole wall and travels back to the sensor where it is recorded [18]. Both peak amplitude and travel time data are retrieved from the reflected signal. The travel time, by difference with the emission time, yields the distance between the sensor and the borehole wall in the sensor azimuth. The sensor rotates continuously during logging (7.5 rotations per sec.) and 180 signals are emitted during one sensor rotation so the angular resolution is 2°.

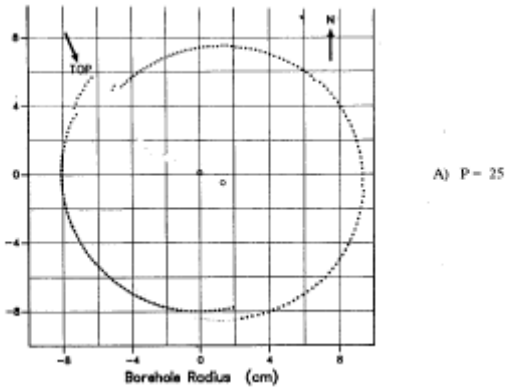

Fig. 6. Determination of the center of a cross section of the well from consecutive ultrasonic shots [9].

Because the tool is never located at the center of the well, a technique has been developed to determine the borehole geometry without knowing where the sensor is [19]. Since the time between two shots is 0.7 msec., it is assumed that the tool has not moved between p consecutive shots (p between 10 and 25). Then these p consecutive shots are used to define the local radius of curvature of the well and therefore the location of its center (fig. 6).

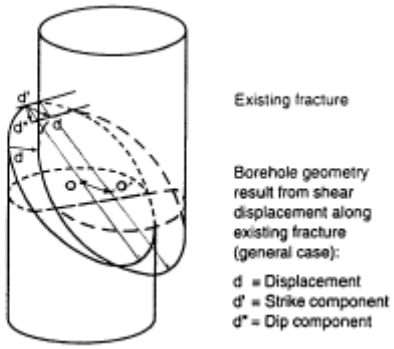

Fig. 7. Determination of slip amplitude from borehole geometry monitoring [9].

When shots in different azimuths yield two different centers, the distance between these centers (OO' on fig. 7) is the projection of the slip in the plane normal to the borehole axis at this location. Resolution of the method is about 0.5 cm and depends on the roughness of the borehole surface.

For 6 different fractures, shear slip have been measured. In particular, a 4.3 cm slip has been detected on a clearly identified inclined plane intersecting the well at a depth of 2925 m, on which some microseismic activity has been observed and precisely relocated through multiplet analysis.

3.2. Confrontation with Multiplet Analysis

When a fault slips at shallow depths over large sections, parts of it move aseismically while parts of it, called asperities, emit seismic signals at repeated time intervals [20, 21]. For such asperities, because the dynamic seismic source function (slip as a function of time) is the same and because the locations of events are very close from each other, the frequency content of the signals are very similar to each other. Such repeated seismic events with similar frequency content are called multiplets.

For each event, the corner frequency and the seismic moment may be interpreted in terms of the size of the source and the amplitude of slip [16, 17]. Very accurate relative source locations may be conducted by cross-correlation of the signals and then the cumulated slip yields an estimate of the amount of slip that has affected the fault at the location of the multiplets.

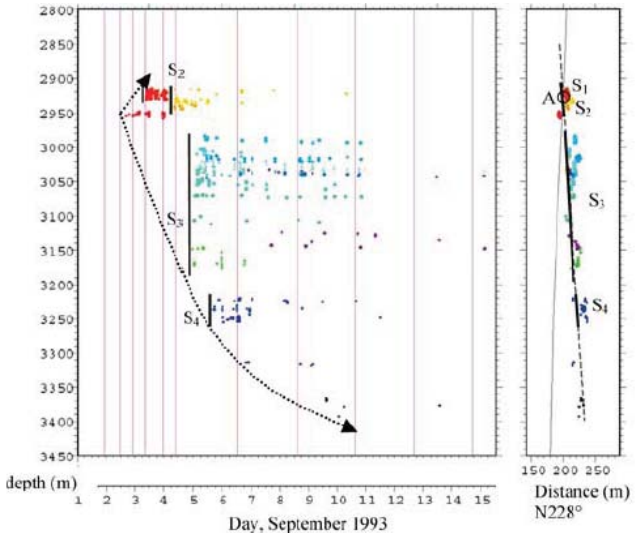

Fig. 8. Location (right) and time of occurrence (left) of multiplets associated with the main creeping fault [15].

A series of 30 multiplets representing a total of 400 events has provided means to identify a planar structure that intersects the well at 2925 ± 25 m, i.e. the very same depth where a slip of 4.3 cm has been measured with UBI logs. The total distance between the most distant multiplets of this structure reaches 400 m, while each source was smaller than 8 m. This is consistent with the

proposition that a 400 m large surface is creeping but the creeping surface involves some local asperities that slip dynamically occasionally, thus illuminating the creeping slipping surface.

Interestingly, Bourouis and Bernard [15] found that most of the asperities support a cumulated slip of a few centimeters (with mean value equal to 4 cm), consistent with the direct borehole observation from UBI logs. However for 3 events, cumulated slip was found to be larger than 10 cm, and even reached 20 cm for one of them. These large values are attributed possibly to directivity effects but also possibly to variability in the slip rate for the corresponding asperity.

4. INDIRECT EVIDENCE OF LARGE SCALE ASEISMIC MOTIONS INDUCED BY THE 2000 GPK2 HYDRAULIC STIMULATION

In 2000, some 23,400 m^3 of water were injected in borehole GPK2 for stimulating the reservoir between 4,400 and 5,000 m (open hole section of the well). Stimulation proceeded with a stepped increase in flow rate, as shown on figure 9.

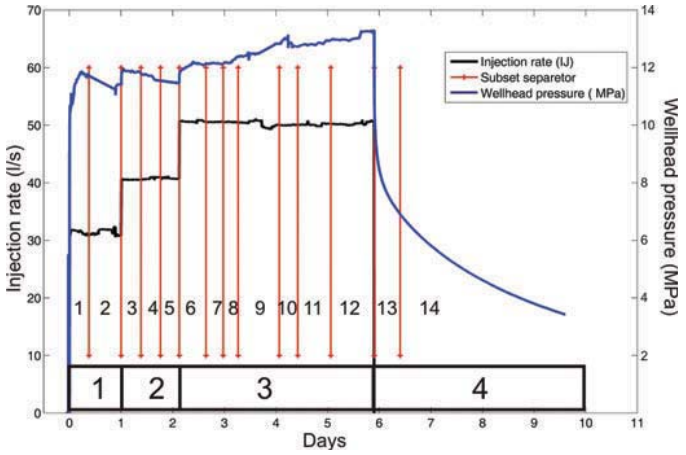

Fig. 9. Hydraulic stimulation of well GP2. Top curve is well head pressure (in MPa) lower curve is flow rate (in l/s=10^{-3} m^3/s); abscissa is time in days. Vertical lines outline periods for which the P waves velocity field has been determined by tomography [22].

Whilst the pressure initially decreased during each of the constant flow rate periods, it started to increase during the last (third) stimulation period after about 10,400 m^3 has been injected since the beginning of stimulation. Injection was followed by a 4 days shut-in experiment during which the well was closed and the pressure decrease was monitored.

Induced seismicity was monitored with a downhole monitoring system integrated within a surface network [10], as already mentioned. The downhole monitoring system was somewhat similar to that used for the 1993 GPK1 stimulation with an additional downhole 4 components station. The surface network included the three permanent 3 components stations and fourteen stations deployed only during stimulations. 8 of them involved only one vertical component with continuous recording but five 3 components stations were recording data only upon triggering.

4.1. Results of Pwave Tomography

About 14,000 events have been located thanks to the downhole network while only 11,000 have been located with the surface network. For some 7,215 events, at least eight P wave arrivals were observed together with three S waves arrivals. However, on average for these events, location was determined from twelve P wave arrivals and five S wave arrivals.

These data were used to solve simultaneously Vp and Vs velocity fields together with the event locations [22] with a code developed by Zhang and Thurber [23]. The horizontal nodes spacing for the tomography was 250 m, near the center of the grid (3.5 km x 3.5 km). But, with this method, the grid structure as well as the a priori input parameters for the velocity field may affect the outcome of the tomography. To limit this bias, the WAM (Weighted Average Model) method [24] was used to determine the best solution for the velocity fields. For this purpose twelve different inversions were run with a grid rotated by 30° with respect to the previous one and an additional three models were investigated with the grid at different depth levels.

This processing was applied to fourteen different data sets chosen so as to coincide either with uniform water injection conditions or to include periods just after water injection parameters had been modified, as indicated on figure 9.

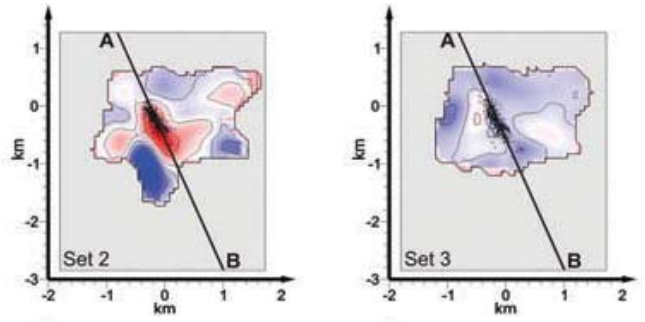

Fig. 10. Comparison of P wave velocity field at 4.6 km, for sets nb 2 and 3. (Horizontal projection) [22]

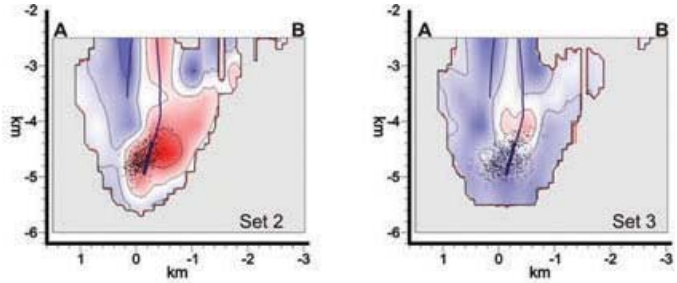

Fig. 11. Comparison of P wave velocity field at 4.6 km, for sets nb 2 and 3. (Vertical projection) [22].

Hence sets 1, 3, and 6 correspond to periods just after injection flow rate has been raised. Periods 13 and 14 correspond to shut in periods. The smallest data set includes 240 events (set nb 5) whilst the largest one includes 780 events (set nb 9).

Figures 10 and 11 illustrate the variation in P wave velocity field as observed between set 2 (second half of 30 l/s pumping period) and set 3 (beginning of 40 l/s pumping period, just after the well head pressure rose 1 MPa). Whilst at the end of set 2 water percolation is decreasing the P wave velocity in the vicinity of the well, this anomaly disappears for set nb 3, just after the pressure has been raised. Calo et al [22] have shown that this change in velocity field occurs within less than 2 hours and is interpreted as a change in effective stress within the rock mass.

But the size of volume affected by the change in velocity is larger than 1 km^3, a volume much larger than that in which the flow rate variation may have induced a change in pore pressure (the rock mass permeability has been evaluated to be in the 10^{-17} - 10^{-16} m^2 range [25]). It is considered that the change in effective stress results from a change in total stress caused by a slip along some fractures or faults. But no significant seismic event with magnitude compatible with these dimensions has been detected. It is concluded that the slip has been sufficiently slow to get undetected with the short period seismic monitoring network.

4.2. Micoseismic locations during Injection and Shut-in Periods

As shown of figure 12, the geometry of the seismic cloud has changed over time. Whilst it outlined a single planar structure that gets thicker and thicker as injection proceeds, it images a fault network during shut-in.

By comparison with the growth of the seismic cloud observed during the 1993 GPK1 stimulation, it is proposed that the growth of the cloud during stimulation was associated with the development of a fresh large scale shear zone, whilst percolation occurred within the initial natural fracture network when the borehole pressure dropped after shut-in. However proper modeling is required for validating this proposition.

5. THE FOUR MECHANISMS OF WATER DIFFUSION IN FRACTURED ROCK MASSES

Figures 5 and 12 outline four different schemes for the growth of the seismic cloud during fluid injections.

5.1. Hydraulic diffusivity in an elastic porous medium

When pressure was raised initially in the open-hole section of the wells, it induced a pore pressure increase in the rock mass that varied with time. As a consequence, the ratio between the maximum differential stress (σ_1–σ_3) and the effective minimum stress (σ_3–P_0) at a given location (σ_1 and σ_3 are respectively the maximum and the minimum principal stress and P_0 is the local pore pressure) increased with time depending on the distance with respect to the location of the fluid source. It is well known from laboratory experiments that when the axial load acting on a rock sample under constant confining pressure increases, some acoustic emissions are generated, even though the rock remains within its elastic domain. This is known as the Kaiser effect [26]. Because the pore pressure variation in the formation depends on the rock mass diffusivity, it has been proposed to interpret the rate of growth of the seismic cloud in terms of rock mass hydraulic diffusivity [25]. However, Cornet et al. [5] have shown that this proposition is valid only as long as the rock remains within its elastic domain. For larger pore pressure variations, large-scale macroscopic failure mechanisms are generated, the growth rate of which controls that of the seismic cloud.

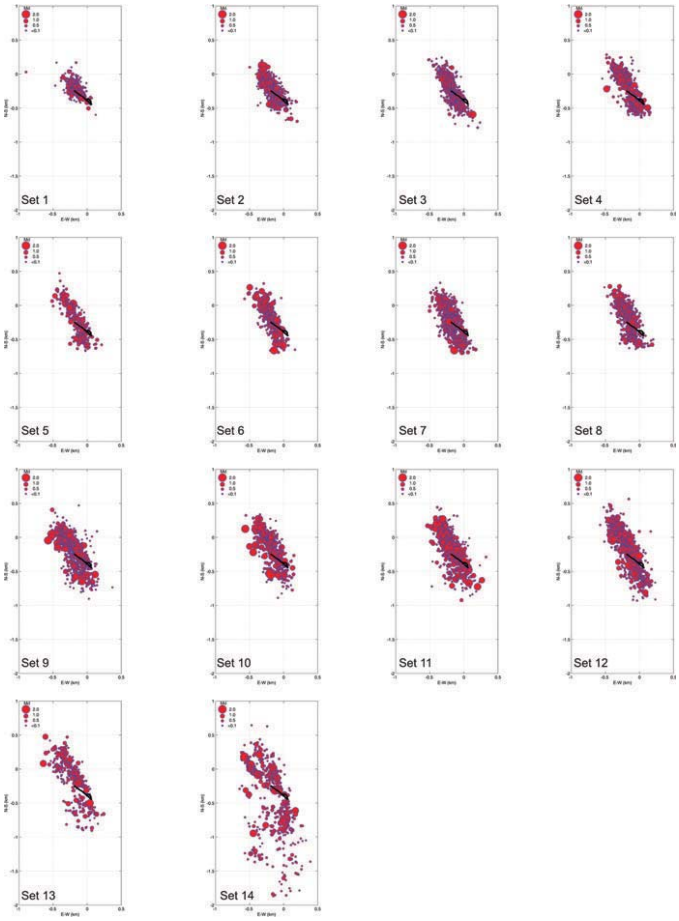

Figure 12: Shape of the microseismic cloud during the various sets defined on figure 9 for the GPK2 stimulation [22]. Events are located within the 4 -5.2 km depth range.

5.2. Slip along preexisting fractures versus fresh shear zone development

On figures 5 (b and d) and figure 12 (sets 13 and 14), the microseismic activity outlines zones with various orientations away from the injection wells. These are

interpreted as preexisting fractures, which have slipped because of the local increase in pore pressure reducing the effective normal stress supported by these features. But the large scale structure outlined close to the injection well on figure 5d, and even more so for sets 1 through 12 of figure 12, outlines a major planar structure that is interpreted as a fresh shear zone. Its orientation is characterized by a Coulomb failure criterion as defined for this rock mass (both structures are inclined 20 to 25° to the maximum principal stress orientation).

Although proper modeling remains to be conducted, the change of growth geometry of the seismic cloud observed between sets 1 to 12 on the one hand and sets 13-14 on the other hand, for the GPK2 stimulation, is considered to be related to the magnitude of the local fluid pressure with respect to the normal stress acting on the large scale shearing structure.

5.3. Hydraulic fracturing

When the fluid pressure gets larger than the local minimum principal stress magnitude, it generates a hydraulic fracture perpendicularly to the minimum principal stress direction. However, close analysis of microseismic sources [12] indicates repeating tensile sources at the same location (tensile source for the multiplets) even though the front of the cloud is quite distant. This mechanism has been interpreted as an en-echelon mode I fracturing process somewhat similar to that of Hill cracks described for volcanic dykes [27].

6. CONCLUSIONS

Results from hydraulic stimulations on the one hand between 2850 m and 3500 m in the well GPK1 and on the other hand in the well GPK2 between 4500 m and 5000 m have induced both seismic and non seismic motions. But whilst the dimensions of the seismic sources are in the 10's of meters range, that of aseismic motions is in the few 100 m range.

Interestingly, the largest seismic events that have been observed at Soultz, but also in Basel (Switzerland) after a similar stimulation had been conducted, occur during shut-in, after the pore pressure has dropped significantly. It is considered that only when aseismic motion has been well understood and is properly monitored will it be possible to optimize stimulation procedures so as to keep the seismic activity at an acceptable level.

ACKNOWLEDGEMENTS

The author would like to thank the International Energy Agency/Geothermal Implementing Agreement and the US Department of Energy for their support of this paper which he trusts encourages international cooperation on topics being pursued by Annex VII, Advanced Geothermal Drilling and logging Technologies. Suggestions by Seid Bourouis are also gratefully acknowledged.

REFERENCES

1. Baria, R., J. Baumgartner, A. Gérard, R. Jung, and J. Garnish. 1999. European HDR research Program at Soultz-sous-Forêts (France) 1987-1996, *Geothermics.* **28**, 655–669

2. Genter, A., D. Fritsch, N. Cuenot, J. Baumgartner and J.J. Graff. 2009. Overview of the current activities of the European EGS project: from exploration to electricity production, in *Proceedings 34TH Workshop on Geothermal Energy*, SGP-TR-187, Stanford University, California.

3. Cornet, F. H., and R. Jones. 1994. Field evidences on the orientation of forced water flow with respect to the regional principal stress directions. in *Proc. 1st North Amer. Rock Mech. Symp. Austin (Texas)* (Nelson and Laubach, eds.) 61–69 Rotterdam. Balkema.

4. Berard, T. and F. H. Cornet. 2003. Evidence of thermally induced borehole elongation: A case study at Soultz, France, *Int. J. Rock Mech. Min. Sci.* **40**, 1121–1140.

5. Cornet, F.H., T. Berard and S Bourouis. 2007. How close to failure is a natural granite rock mass at 5 km depth, *Int. J. Rock Mech. Min. Sci.* **44**, 47–66.

6. Valley, B. and K. F. Evans. 2007. Stress State At Soultz-Sous-Forêts to 5 km depth from wellbore failure and hydraulic observations, in *Proc. 32nd Workshop on Geothermal Reservoir Engineering,* Stanford University, Stanford, CA, 2007

7. Dorbath L., K. Evans, N. Cuenot, B. Valley, J. Charléty and M. Frogneux. 2010. The stress field at Soultz-sous-Forêts from focal mechanisms of induced seismic events: cases of the well GPK2 and GPK3. – *C. R. Geosciences*, **342**, 600-606.

8. Jones, R.H., A. Beauce, A. Jupe, H. Fabriol and B.C. Dyer, 1995. Imaging induced micro-seismicity during the 1993 injection tests at Soultz-sous-Forêts. in: *Proc. World Geothermal Congress, Florence, Italy.* 2665–2669. International Geothermal Association

9. Cornet, F.H., J. Helm, H. Poitrenaud and A. Etchecopar. 1997. Seismic and aseismic slips induced by large scale fluid injections. *Pure appl. Geophys.*, **150**, 563–583.

10. Cuenot, N., C. Dorbath, and L. Dorbath. 2008. Analysis of the microseismicity induced by fluid injection in the Hot Dry Rock site of Soultz sous-Forêts (Alsace, France): implications for the characterization

of the geothermal reservoir properties, *Pure appl. Geophys.*, **165**, 797–828.

11. Evans, K. F., T. Kohl, R. J. Hopkirk, and L. Rybach. 1996. Studies of the Nature of Nonlinear Impedance to Flow within the Fractured Granitic Reservoir at the European Hot Dry Rock Project Site at Soultz-sous-Forêts, France, *Bundesamt für Bildung und Wissenschaft, Projekt 93.0010—Final Report*;144 pp; Swiss Federal Inst. of Tech, Institute of Geophysics Zürich.

12. Sileny J, L. Eisner, D.P. Hill and F.H. Cornet; 2009 Non double couple mechanisms of microearthquakes induced by hydraulic fracturing; *J. Geophys. res.,* **114**, B08307.

13. Secor, D.T. and D.D. Polard, 1975. On the stability of open hydraulic fractures in the earth's crust *Geophys. res. let*., **2**, 510-513.

14. Fehler M, L House and H. Kaieda 1987. Determining planes along which earthquakes occur: method and application to earthquakes accompanying hydraulic fracturing; *J. Geophys. res.*, **92**: 9407-9414.

15. Bourouis, S and P. Bernard, 2007. Evidence for coupled seismic and aseismic fault slip during water injection in the geothermal site of Soultz (France), and implications for seismogenic transients. *Geophys. J. Int.* **169,** 723-732.

16. Brune, J., 1970. Tectonic stress and the spectra of seismic shear waves from earthquakes, *J. geophys. res.,* **75,** 4997–5009.

17. Brune, J., 1971. correction. *J. geophys. res.,* **76,** 5002.

18. Zemanek, J., E. Glenn, C. J. Norton, and R. L. Cardwell. 1970, Formation Evaluation by Inspection with a Borehole Televiewer, *Geophys.* **35**, 254–269.

19. Hayman, A., P. Parent, P., Cheung and P. Verges, 1994, Improved Borehole Imaging by Ultrasonics, *Soc. Petr. Eng. Paper 28 440.*

20. Poupinet G., W. L. Ellsworth and J. Frechet, 1984. Monitoring Velocity Variations in the Crust Using Earthquake Doublets: An Application to the Calaveras Fault, California; *J. Geophys. res.,* **89**, 5719-5731

21. Nadeau, R. and T.V., McEvilly, 1999. Fault slip rates at depth from recurrence intervals of repeating microearthquakes, *Science,* **285,** 718–721.

22. Calo M., C. Dorbath, F.H. Cornet and N. Cuenot; 2011, Large scale aseismic motion identified through 4D P-wave tomography; *Geophys. J. Int.* **186**, 1295-1314;

23. Zhang, H. and C.H. Thurber, 2003. Double-difference tomography: the method and its application to the Hayward fault, California, *Bull. seism.Soc. Am.*, **93**, 1175–1189.

24. Calo, M., C. Dorbath, D.. Luzio, S.G. Rotolo, and G. D'Anna, 2009. Local earthquakes tomography in the southern Tyrrhenian region: geophysical and petrological inferences on subducting lithosphere, in *Subduction Zone Geodynamics, Frontiers in Earth Sciences*, pp. 85–99, eds Lallemand, S. & Funiciello, F., Springer-Verlag, Berlin.

25. Shapiro S.A., E. Rothert, V. Rath and J. Rindschwentner, 2002. Characterization of fluid transport properties of reservoirs using induced microseismicity. *Geophysics* **67**, 212-220

26. Holcomb D.J., 1993. General theory of the Kaiser effect. *Int J Rock Mech Min Sci Geomech Abstr* **30**:929–935

27. Hill D.P. 1977. A model for earthquake swarms. *J Geophys Res* **82**:1347–1352